

**SLOVAK UNIVERSITY OF TECHNOLOGY  
IN BRATISLAVA  
FACULTY OF ELECTRICAL ENGINEERING AND INFORMATION TECHNOLOGY**

**Ing. Anežka Chovancová**

**Dissertation Thesis Abstract**

**CONTROL OF 4-ROTOR FLYING PLATFORM**

**to obtain the Academic Title of  
„doktor“ („philosophiae doctor“, abbreviated as „PhD.“)**

**in the doctorate degree study programme  
Robotics and cybernetics**

**in the field of study  
9.2.7. Cybernetics**

**Bratislava, August 2017**

Dissertation Thesis has been prepared in the full-time, attendance method form at Institute of Robotics and Cybernetics of Faculty of Electrical Engineering and Information Technology in Slovak University of Technology in Bratislava.

**Submitter:** **Ing. Anežka Chovancová**

Institute of Robotics and Cybernetics  
Faculty of Electrical Engineering and Information Technology  
Slovak University of Technology in Bratislava, Ilkovičova 3, 812 19 Bratislava

**Supervisor:** **doc. Ing. František Duchoň, PhD.**

Institute of Robotics and Cybernetics  
Faculty of Electrical Engineering and Information Technology  
Slovak University of Technology in Bratislava, Ilkovičova 3, 812 19 Bratislava

**Readers:** **prof. Ing. Aleš Janota, PhD. EurIng**

Department of Control and Information Systems  
Faculty of Electrical Engineering  
University of Žilina, Univerzitná 1, 010 26 Žilina

**prof. Ing. Michal Kelemen, PhD.**

Department of Mechatronics  
Faculty of Mechanical Engineering  
Technical University of Košice, Letná 9, 040 01 Košice

**Dissertation Thesis Abstract was sent:**

**Dissertation Thesis Defence will be held on:**

**at** Faculty of Electrical Engineering and Information Technology STU in Bratislava, Ilkovičova 3, Bratislava in room D424.

prof. Dr. Ing. Miloš Oravec  
Dean of FEI STU

# Content

Introduction .....	4
Goals of the dissertation thesis .....	4
1 Mathematical Model of Quadrotor .....	5
2 Test stands .....	8
2.1 Design of test bed for identification of static and dynamic characteristics of the actuator.....	8
2.2 Design of test stand for testing purposes.....	10
3 Identification of parameters of quadrotor.....	11
4 State space estimator and disturbance observer.....	12
4.1 State space estimator .....	13
4.2 Disturbance observer.....	14
5 Simulation.....	15
5.1 Simulation parameters and parameters of designed controllers .....	15
5.2 Trajectory tracking without the external disturbance.....	17
5.3 Trajectory tracking with the occurrence of the external disturbance.....	20
6 Experimental results.....	23
6.1 Implementation of control algorithm into real platform .....	23
6.2 HMI for data collection and command execution.....	24
6.3 Verification of proposed control algorithms .....	24
6.3.1 Parameters of designed controllers applied to real platform .....	25
6.3.2 Tracking desired sequence of orientation .....	26
Conclusion.....	31
Main contribution of the dissertation thesis .....	32
References .....	33
Overview of author's publications .....	34

## **Introduction**

The aim of this thesis is to design and verify various control techniques for a quadrotor using a quaternion representation of attitude. All attitude controllers use a quaternion error to compute control signals for motors. The quaternion error is calculated from an actual quaternion and a desired quaternion obtained from a position controller. Attitude and position control laws are computed using a PD, LQR and backstepping control techniques.

All combinations of controllers are verified by simulation. Parameters of the actuator of the quadrotor are experimentally determined using a test bed which design and construction form part of this thesis. We add noise, apply an actuator restriction and use a different sampling period for position and attitude feedback signals to get the simulation closer to real conditions.

Moreover, external disturbances are implemented into the simulation; hence a disturbance observer along with a position estimator will be designed to improve the performance of the presented controllers.

The simulated performance of all combinations of controllers is evaluated using various quality indicators, such as the integral of absolute errors and total thrust, settling times and also maximum overshoots when external disturbance is applied. Some of the controllers exhibit very similar behaviour, so the three best controllers are chosen for each scenario used in the simulation.

Designed attitude controllers are implemented into microcontroller on the control board of the real quadrotor. The attitude of the quadrotor is calculated using angular velocities read from MPU9150 IMU. The application for PC is created to establish connection to the control board of the quadrotor. The attitude setpoints and also control signals are transferred to the quadrotor via Bluetooth device from PC.

The attitude controllers are verified using test stand created for this purpose. The performance of controllers is evaluated using various quality indicators, such as the integral of absolute quaternion error, integral of the absolute desired torque and maximum absolute variation of the quaternion.

## **Goals of the dissertation thesis**

1. Design and construction of the test bed and test stand used to parameter identification of the quadrotor and to test proposed attitude controller of the quadrotor.
2. Design of various attitude and position controllers with the occurrence of the external disturbance.

3. Selection of the best controller according to the quality of regulation, power consumption and the complexity of the control algorithm. The controller selection is made out of simulations of the non-linear model of the quadrotor.
4. Implementation of the proposed attitude control algorithm into the real flying platform and evaluation of the quality of the control algorithm using a proposed test stand.

## 1 Mathematical Model of Quadrotor

This section will focus on derivation of mathematical model of quadrotor using Newton-Euler equations. A quaternion was chosen for representation of attitude of the quadrotor.

The variation of the position and orientation is reached by varying the angular speed of the particular rotor. Motors of quadrotor are placed in vertices of a square at distance  $l$  from the centre of quadrotor. This configuration provides torque control in the axes  $z_B$ , i.e. yaw control, without other additional units.

Henceforth for simplicity the following notation for time dependent variables will be used:  $x$  instead of  $x(t)$ .

A quaternion defines a single rotation  $\alpha$  around an axis  $\mathbf{r}$ . The notation of the rotation is given as a hyper complex number of rank 4 composed of the scalar  $q_\alpha \in \mathbb{R}$  and the vector  $\mathbf{q}_r \in \mathbb{R}^3$ . The quaternion formulation is given by equation (1.1), where  $\alpha$  and  $\mathbf{r}$  stand for the angle and axis of the rotation, respectively. The rotation is clockwise if our line of sight points in the same direction as  $\mathbf{r}$  [2], [3], [4], [5].

$$\mathbf{q} = \left[ \cos \frac{\alpha}{2} \quad \mathbf{r}^T \sin \frac{\alpha}{2} \right]^T = [q_\alpha \quad \mathbf{q}_r]^T = [q_\alpha \quad q_x \quad q_y \quad q_z]^T \quad (1.1)$$

Given two rotations  $\mathbf{q}_1$  and  $\mathbf{q}_2$ , the combined rotation is expressed by their multiplication  $\mathbf{q}_1 \circ \mathbf{q}_2$  corresponding to the rotation  $\mathbf{q}_2$  followed by the rotation  $\mathbf{q}_1$ . Moreover  $\mathbf{q}^n$  is a rotation by  $n$  times the angle around the same axis as  $\mathbf{q}$ . The rotations are non-commutative, hence the quaternion multiplication is non-commutative either, i.e.  $\mathbf{q}_1 \circ \mathbf{q}_2 \neq \mathbf{q}_2 \circ \mathbf{q}_1$ .

$$\mathbf{q}_1 \circ \mathbf{q}_2 = \begin{bmatrix} q_{\alpha 1} q_{\alpha 2} - \mathbf{q}_{r 1}^T \mathbf{q}_{r 2} \\ q_{\alpha 1} \mathbf{q}_{r 2} + q_{\alpha 2} \mathbf{q}_{r 1} + \mathbf{q}_{r 1} \times \mathbf{q}_{r 2} \end{bmatrix} \quad (1.2)$$

Given a unit quaternion  $\mathbf{q}$ , the multiplication of the quaternion  $\mathbf{q}$  and its inverse is commutative, i.e.  $\mathbf{q} \circ \mathbf{q}^{-1} = \mathbf{q}^{-1} \circ \mathbf{q}$  and is equal to  $[1 \quad 0 \quad 0 \quad 0]^T$ .

The three-dimensional rotation of any vector is given as a quaternion multiplication on the left by the unit quaternion  $\mathbf{q}$  and on the right by its conjugate  $\mathbf{q}^*$ . This mathematical operation can be rewritten as a multiplication of the matrix  $\mathbf{R}_q$  and the abovementioned vector. Because we are rotating a vector, only the vector part from the rotation matrix is extracted as can be seen in equation (1.3), where  $q_{r \times}$

stands for a skew-symmetric matrix. The rotation matrix  $\mathbf{R}_q$  is orthogonal; therefore the expression  $\mathbf{R}_q^{-1} = \mathbf{R}_q^T$  is true [12].

$$\begin{aligned} \mathbf{R}_q &= (q_\alpha \mathbf{I} + \mathbf{q}_{r \times})^2 + \mathbf{q}_r \mathbf{q}_r^T = (q_\alpha^2 - \mathbf{q}_r^T \mathbf{q}_r) \mathbf{I} + 2q_\alpha \mathbf{q}_{r \times} + 2\mathbf{q}_r \mathbf{q}_r^T \\ &= \begin{bmatrix} q_\alpha^2 + q_x^2 - q_y^2 - q_z^2 & 2(q_x q_y - q_z q_\alpha) & 2(q_x q_z + q_y q_\alpha) \\ 2(q_x q_y + q_z q_\alpha) & q_\alpha^2 - q_x^2 + q_y^2 - q_z^2 & 2(q_y q_z - q_x q_\alpha) \\ 2(q_x q_z - q_y q_\alpha) & 2(q_y q_z + q_x q_\alpha) & q_\alpha^2 - q_x^2 - q_y^2 + q_z^2 \end{bmatrix} \end{aligned} \quad (1.3)$$

The derivative of a quaternion is given by the quaternion multiplication of the quaternion  $\mathbf{q}$  and the angular velocity of the system  $\boldsymbol{\eta}$ , which in this case is the quadrotor.

$$\dot{\mathbf{q}} = \begin{bmatrix} \dot{q}_\alpha \\ \dot{\mathbf{q}}_r \end{bmatrix} = \frac{1}{2} \mathbf{q} \circ \begin{bmatrix} 0 \\ \boldsymbol{\eta} \end{bmatrix} = \frac{1}{2} \begin{bmatrix} 0 & -\boldsymbol{\eta}^T \\ \boldsymbol{\eta} & -\boldsymbol{\eta}_\times \end{bmatrix} \begin{bmatrix} q_\alpha \\ \mathbf{q}_r \end{bmatrix} \quad (1.4)$$

When designing a controller it is very important to define a quaternion error. The quaternion error is given as the quaternion multiplication of the conjugate of the actual quaternion  $\mathbf{q}$  and the desired quaternion  $\mathbf{q}_d$ .

$$\mathbf{q}_{err} = \mathbf{q}^* \circ \mathbf{q}_d = \begin{bmatrix} q_\alpha q_{\alpha d} + \mathbf{q}_r^T \mathbf{q}_{rd} \\ q_\alpha \mathbf{q}_{rd} - q_{\alpha d} \mathbf{q}_r - \mathbf{q}_r \times \mathbf{q}_{rd} \end{bmatrix} \quad (1.5)$$

The quaternion error is the rotation that should be performed to reach the desired orientation.

In this thesis the Newton–Euler equations is derived, while assuming that the quadrotor is a rigid body and the centre of gravity coincides with the body-fixed frame origin.

While developing mathematical model of the quadrotor, three coordinate frames are considered: the non-moving inertial frame  $\mathbf{E}_I$ , the body-fixed frame  $\mathbf{E}_B$  depicted in Figure 1.1.

Assuming a symmetric mass distribution of the quadrotor, the statement  $\forall i \neq j \Rightarrow I_{ij} = 0$  is true and so the inertia matrix of the quadrotor  $\mathbf{I}_q$  [kg·m<sup>2</sup>] is a diagonal matrix. [6].

The thrust generated by rotor  $i$  given by equation (1.6) is proportional to the square of the angular speed of the rotor and the thrust constant  $k_T$  [kg·m]. The thrust constant is formed of the air density  $\rho$  [kg·m<sup>-3</sup>], the radius of the propeller  $r$  [m], and the thrust coefficient  $c_T$ , that depends on blade rotor characteristics, such as number of blades, chord length of the blade, and cube of the rotor blade radius [6], [7], [8].

$$F_i = c_T \rho \pi r^4 \omega_i^2 = k_T \omega_i^2 \quad (1.6)$$

The torque developed around the rotor axis is given by equation (1.7) as the product of the square of the angular speed and the drag coefficient  $k_D$  [kg·m<sup>2</sup>]. The drag coefficient depends on the same factors as the thrust constant and even on the angular acceleration of rotor  $i$  multiplied by the moment of inertia of the rotor  $J_r$  [3], [6], [7]. Normally, the effect of the angular acceleration of rotor  $\dot{\omega}_i$  is very small; therefore it can be neglected [12].

$$D_i = c_D \rho \pi r^5 \omega_i^2 + J_r \dot{\omega}_i \approx k_D \omega_i^2 \quad (1.7)$$

The torque created around a particular axis by particular rotors with respect to the body-fixed frame is defined in equation (1.8), where  $\Phi_i$  [rad] denotes the multiple of the angle between the arms of the quadrotor [8].

$$\boldsymbol{\tau} = \begin{bmatrix} \tau_x \\ \tau_y \\ \tau_z \end{bmatrix} = \begin{bmatrix} l \sum_{i=1}^4 \sin \Phi_i \mathbf{F}_i \\ -l \sum_{i=1}^4 \cos \Phi_i \mathbf{F}_i \\ \sum_{i=1}^4 (-1)^i \mathbf{D}_i \end{bmatrix} = \begin{bmatrix} lk_T(\omega_2^2 - \omega_4^2) \\ lk_T(\omega_1^2 - \omega_3^2) \\ k_D(-\omega_1^2 + \omega_2^2 - \omega_3^2 + \omega_4^2) \end{bmatrix} \quad (1.8)$$

The thrust  $T$  [N] of the quadrotor is always aligned with the  $z$  axis in the body-fixed frame and it is given as a sum of all thrusts  $F_i$  generated by rotors.

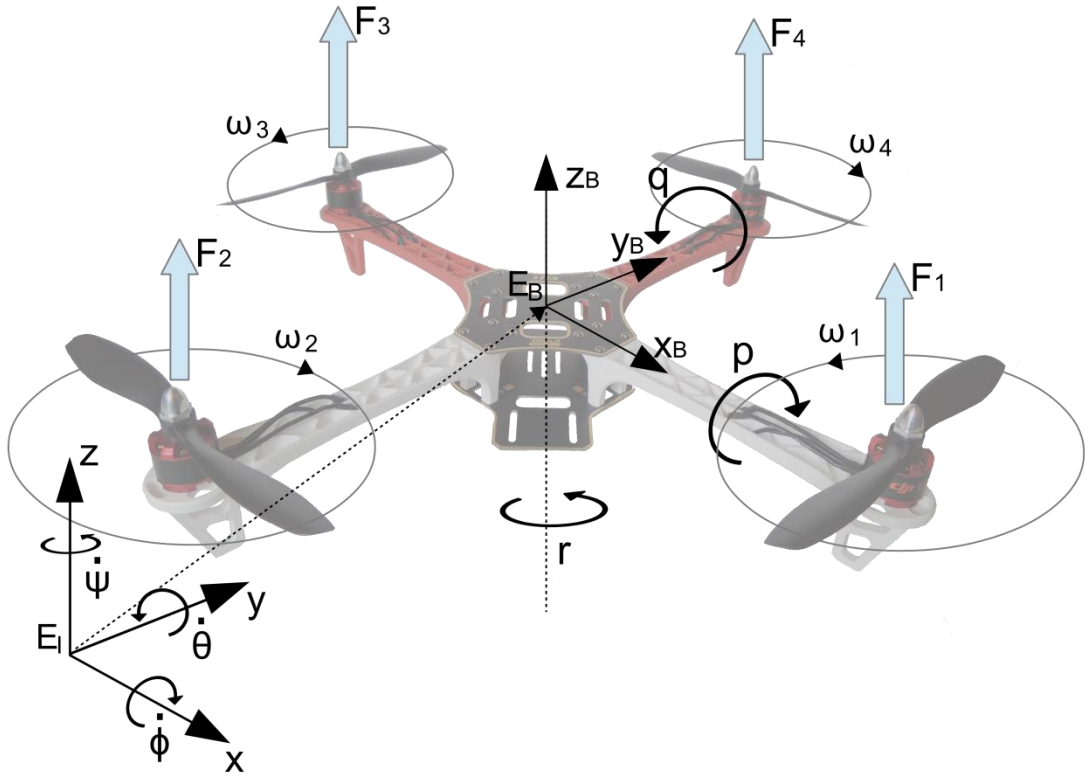


Figure 1.1 Inertial and body-fixed frame of the quadrotor.

In general, the attitude of the quadrotor is described in the body-fixed frame and the position of the quadrotor is defined in the inertial frame.

The equation describing the rotation of the quadrotor with respect to the body-fixed frame is given by equation (1.9). It involves the torque developed by all four rotors  $\boldsymbol{\tau}$  [N·m], the centripetal torque  $\boldsymbol{\tau}_c$ , the gyroscopic torque  $\boldsymbol{\tau}_g$  and the disturbance torque  $\boldsymbol{\tau}_{dist}$  that contains, among other things, an aerodynamic drag [1], [3], [7], [8], [9], [12], [13].

$$I_q \dot{\eta} = \tau - \eta \times I_q \eta - J_r \sum_{i=1}^4 \eta \times \begin{bmatrix} 0 \\ 0 \\ (-1)^{i+1} \omega_i \end{bmatrix} - \tau_{dist} \quad (1.9)$$

The non-linear model of translation with respect to the inertial frame consists of the force given by the acceleration of quadrotor with the mass  $m$  [kg], total thrust  $T$  rotated using the rotation matrix  $R_q$ , the gravity force and the disturbance force [3], [9].

$$m \ddot{\xi} = R_q \begin{bmatrix} 0 \\ 0 \\ T \end{bmatrix} - \begin{bmatrix} 0 \\ 0 \\ mg \end{bmatrix} - F_{dist} \quad (1.10)$$

## 2 Test stands

In this chapter the test bed for identification of the actuator and test stand designed for testing control algorithms will be described. The test bed will be used to identify static and dynamic characteristics of the actuators. The test stand will be used to debug program written to microcontroller memory when using a real quadrotor and protect quadrotor and surroundings.

### 2.1 Design of test bed for identification of static and dynamic characteristics of the actuator

In order to identify coefficients of the rotors, namely the thrust coefficient and the drag coefficient, the relation between the force/torque and rotor speed or PWM (Pulse Width Modulation) sent to ESC must be measured.

A low-cost measuring test bed was designed to measure force, torque, battery voltage and current, so that complete identification including motor dynamics can be established. Our design uses only a data acquisition and control board (DAQCB), low-priced binocular beam load cell, incremental encoder and a PC to fully identify the actuator. The approximated price of the designed test bed is 60€.

Mechanical construction of the test bed (Figure 2.1) for measuring thrust consists of a large wooden board, an arm of the quadrotor frame, a binocular beam load cell, an optical sensor and the actuator. Maximum load capacity of the load cell is 5 kg. Its output transfer sensitivity is 1 mV per 1 V of excitation voltage at full load. The binocular beam load cell incorporates a full-bridge configuration of strain gauges. Because of the two holes in the middle of the load cell, it can measure only vertical deformation and the length of the arm is not taken into account during the measurement. The usage of four strain gauges ensures compensation of the unwanted temperature effect on the output signal and increases measuring sensitivity.

An encoder was used to measure the motor speed. For this purpose, the outer side of the motor was covered with a sequence of 22 black and white stripes.

The input-output DAQCB was developed to amplify the output signal from the load cell and to gather other signals. The board connects the object of measurement (ESC, BLDCM, battery) with the

I/O board MF624 from Humusoft. The real advantage of MF624 is its support of the Matlab Simulink environment. A created Simulink model uses the Real Time Toolbox to collect data from the board and to create a setpoint for the ESC.

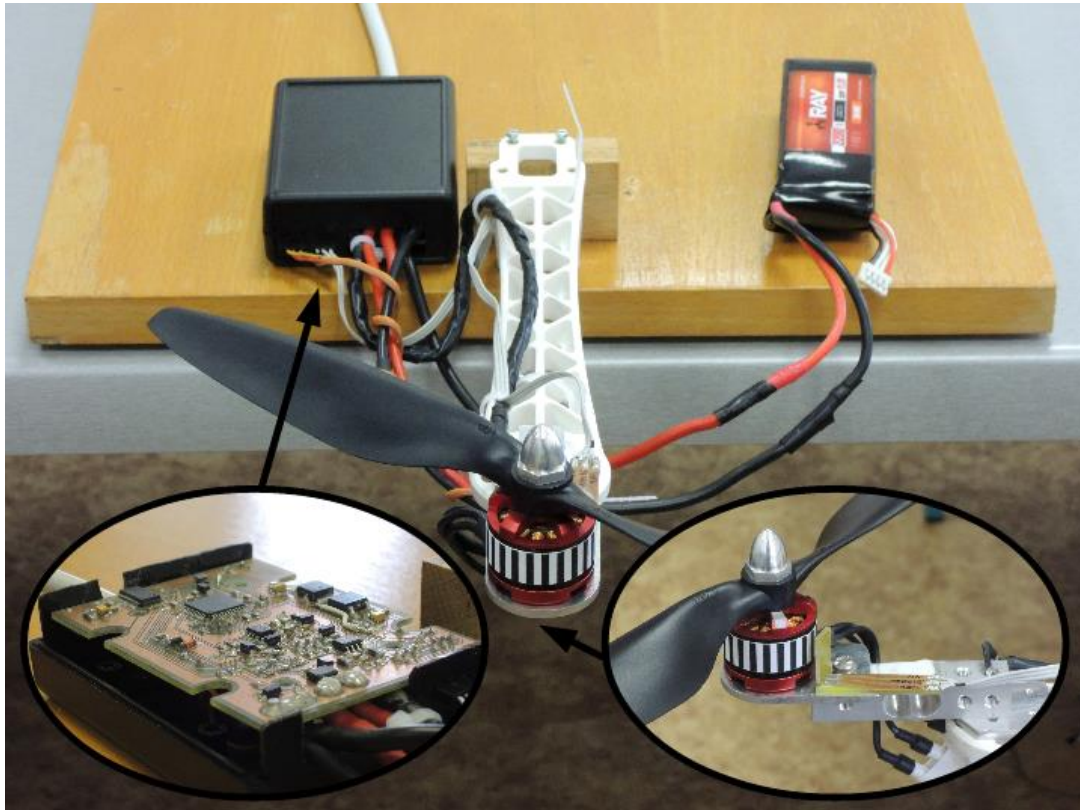


Figure 2.1 Test bed used to identify static and dynamic characteristics of the actuator.

Figure 2.2 shows the block diagram of the created DAQCB. Besides motor speed and thrust, the board also measures battery voltage and current consumed by the ESC and motor. The design of the board allows its use without an external DAQ board in a PC. The heart of the board is an Atmel ATmega16A microcontroller. Using the USB interface, which creates a virtual serial line, the board is able to receive control commands and send measured data. The ATmega16A contains only a 10 bit converter compared to the 14 bit one in the MF624 board, but for the purpose of the identification this resolution is sufficient.

Measurement of the current consumed by the motor is performed using a Hall effect-based linear current sensor IC ACS712. Because of the small resistance (1.2 mΩ), voltage drop and power loss is minimized.

Another function of the microcontroller is the conversion of the control voltage from the MF624 to a PWM signal sent to the ESC using the following equation:

$$p = 1000 + 99.5U_{PWM} \quad (2.1)$$

$U_{PWM}$  is the control voltage and  $p$  [ $\mu$ s] is the pulse width sent to the ESC. Zero power is represented by the value of 1 ms and full power by the value of 2 ms. The PWM signal is calculated with a resolution of 8 bits and sent to the ESC with a refresh rate of 250 Hz.

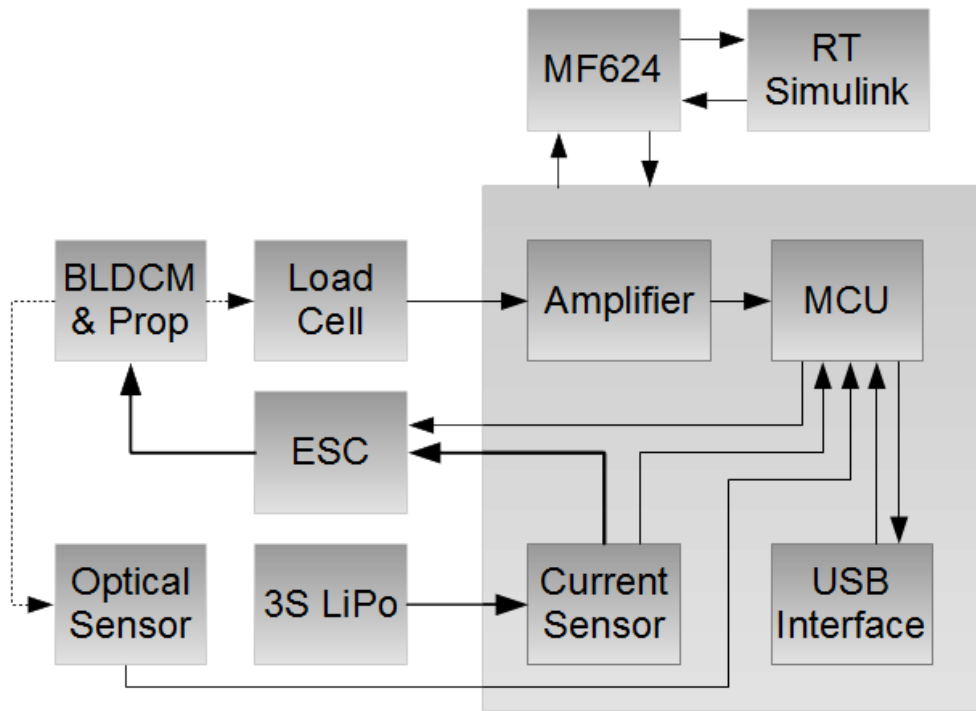


Figure 2.2 Block diagram of the measuring test bed.

## 2.2 Design of test stand for testing purposes

The chapter focuses on designing and building a prototype of test stand which allows us to test the attitude controller in the 3 degrees of freedom.

The test stand comprised of 2 parts, i.e. an unmoving metal part which holds a rotary part which can rotate around all 3 axes. It can be used to mount and therefore to test any VTOL platform which maximum dimension is not greater than 0.75 m including the length of propellers.

Rotary part comprised of carbon tubes and polymer parts including a ball bearings Figure 2.3 part 1, 2 and 3). Magnetic rotary sensors are mounted on these polymer parts and provide us with following measurements: pitch, roll, yaw and their corresponding angular velocities.

VTOL platform, in our case quadrotor, is mounted on a plate with dimension 0.1 m x 0.1 m in the centre of the test stand. The quadrotor can be adjust in  $z$  axis so that the plane of the propellers contains the  $x$  and  $y$  axis of rotation of the test stand.

The module 1 measures roll, module 2 measures pitch and module 3 measures yaw angle. All modules are powered from external source of power supply via cables which are laid inside the carbon tubes.

The transition between moving parts is provided through a rotary contacts. The real prototype is depicted in Figure 2.3. The stand comprised of 4 modules, from which 3 are slaves used to measure

orientation. The function of the 4th master module is to collect data from slave modules and send it to the superior system such as personal computer. Modules communicate between each other via one wire interface. The communication between the superior system and the stand is established via USB interface. A cyclic redundancy check (CRC) was used to ensure that the received data are valid.



Figure 2.3 Prototype of the test stand.

This design of the stand has various advantages in comparison with the stand currently on the market. The main advantage of the stand is that the tested VTOL can rotate in all 3 axes without restriction. We also used an absolute rotary position sensor for the measurement of the orientation. This type of the sensor do not suffer from the drift and provide us with the absolute orientation of the tested VTOL that means that the stand can also be used to calibrate IMU sensor mounted on the VTOL.

Even though we use modern light materials to build out the stand, the moment of inertia around  $x$  axis will have impact on the dynamics of the tested VTOL.

### 3 Identification of parameters of quadrotor

The parameters of the mathematical model of the quadrotor such as an inertia matrix and friction coefficients can be obtained via simple measurements of the weight and the length later used in the calculations. Other parameters such as a thrust and drag coefficients are identified by experiments and some are measured, for example an arm length and total mass of quadrotor.

The moment of inertia can be estimated via calculation using simplified model of the quadrotor which only consists of basic shapes such as a cube, cylinder or a sphere [7], [14] then Steiner's theorem is used to determine the moment of inertia of the quadrotor.

Drag coefficient can be calculated using equation (3.1) where  $C_k$  is a friction coefficient,  $\rho$  is an air density and  $A_i$  is a reference area.

$$K_i = \frac{1}{2} C_k A_i \rho \quad (3.1)$$

The drag coefficient is normally measured using a wind tunnel but because none was available the approximation of the drag coefficient will be calculated using equation (3.1) where the value of the friction coefficient will be 0.5 as it was estimated in [11]. Air density  $\rho$  is equal to 1.2041 kg.m<sup>-3</sup> at temperature equal to 20°C and pressure equal to 101.325 kPa.

Thrust and drag torque are crucial parameters, which can be expressed in relation to the angular speed of the rotor or the pulse width of PWM [10], [7], [9].

All measured values were gained from steady states. The measured signals were current, voltage, thrust and angular speed of the rotor. Signal gained from DAQCB was implemented through Matlab card MF 624 to computer and measured data was imported and processed in Matlab Simulink.

Angular speed of rotor is calculated from data measured with incremental encoder using equation (3.2), where  $imp_i$  is number of impulses in time  $i$ ,  $T_v$  is sample period and  $P_o$  is number of pulses per revolution of the encoding sequence located on the periphery of the rotor:

$$\omega_i = \frac{60(imp_i - imp_{i-1})}{P_o T_v} = \frac{60(imp_i - imp_{i-1})}{22 * 0,01} \quad (3.2)$$

The linear approximation of the thrust of the actuator with respect to the PWM is given by equation (3.3) while the quadratic approximation is given by equation (3.4).

$$F_i = 0.0105p - 12.619 \quad (3.3)$$

$$F_i = 5.083e^{-6}p^2 - 0.0053p - 0.68 \quad (3.4)$$

Linear approximation of the torque of the actuator with respect to the it is given by equation (3.5) while the quadratic approximation is given by equation (3.6).

$$D_i = 2.022e^{-4}p - 0.2336 \quad (3.5)$$

$$D_i = 1.901e^{-7}p^2 - 1.356e^{-4}p - 0.023 \quad (3.6)$$

#### 4 State space estimator and disturbance observer

In this work a state-space estimator for the position and the linear velocity along with the attitude and position disturbance observer are designed in order to reduce the noise and improve the performance when external disturbances are present.

A state-space estimator is used to compute signals that cannot be measured, or to join various noisy signals in order to remove the noise. The presence of noise can lead to various undesirable effects, e.g. a deterioration of the final position with time. Under windy conditions, the DO or the robust controller can be designed to improve the performance of the position tracking.

## 4.1 State space estimator

The state space estimator computes the position and the velocity of quadrotor that are used in the position control. The measured position contains noise, which is even amplified after a derivation when acquiring the linear velocity.

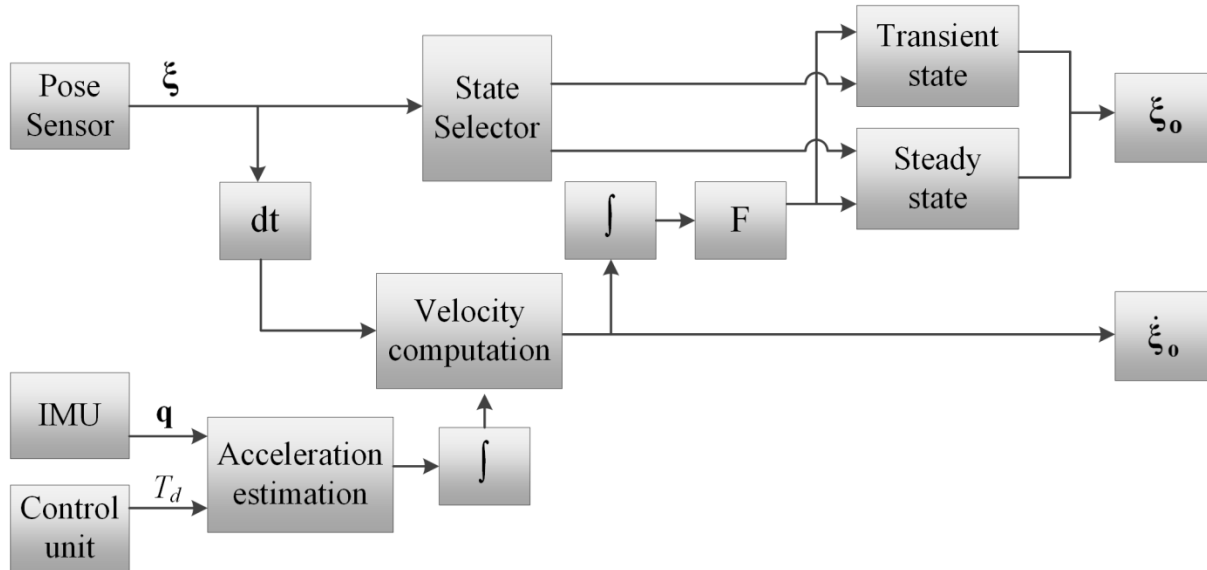


Figure 4.1 Block diagram of the proposed position and linear velocity state space estimator.

The most often used sensor for the position is a GPS module. A common GPS module works at 10 Hz update rate, i.e. new values are obtained every 100 ms.

The goal of the estimator is to acquire both the position and the linear velocity of the quadrotor at 100 Hz rate. The block diagram of the proposed position and linear velocity state space estimator is depicted in Figure 4.1.

The performance of the observer is shown in the Figure 4.2, where the real, measured and the estimated signal of the position and the velocity in the  $z$  axis are compared.

As can be seen in Figure 4.2 the estimated position is tracking the real position in both transient and steady states. The transition between these two states is smooth.

The estimated velocity is not only getting closer to the real value compared to the derivation of the measured position, but also is predicting the slope to the next measured value.

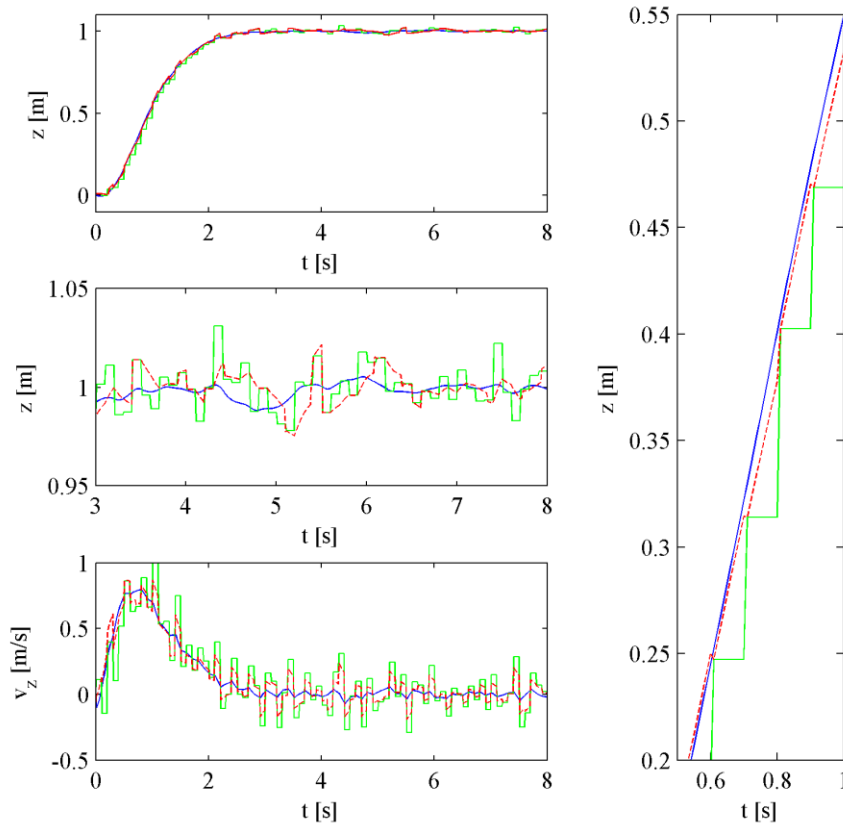


Figure 4.2 An example of the performance of the state space estimator; the blue line represents the real signal, the green line represents the measured signal and the red line represents the estimated signal.

## 4.2 Disturbance observer

The aim of the disturbance observer is to detect and determine the amplitude of the disturbance interpreted as a linear and an angular acceleration. Figure 4.3 shows the block diagram of both observers.

The identification of an external disturbance that is applied at time  $t = 20$  s and disappears at time  $t = 40$  s. The position disturbance corresponds to the force equal to the vector  $[2 \ 2 \ -5]$ . The algorithm identifies the applied disturbance within 1 s and then the calculated value oscillates around the correct value with the maximum amplitude of  $0.12 \text{ m}\cdot\text{s}^{-2}$ . The force is identified in the form of the linear acceleration and implemented to the control algorithm.

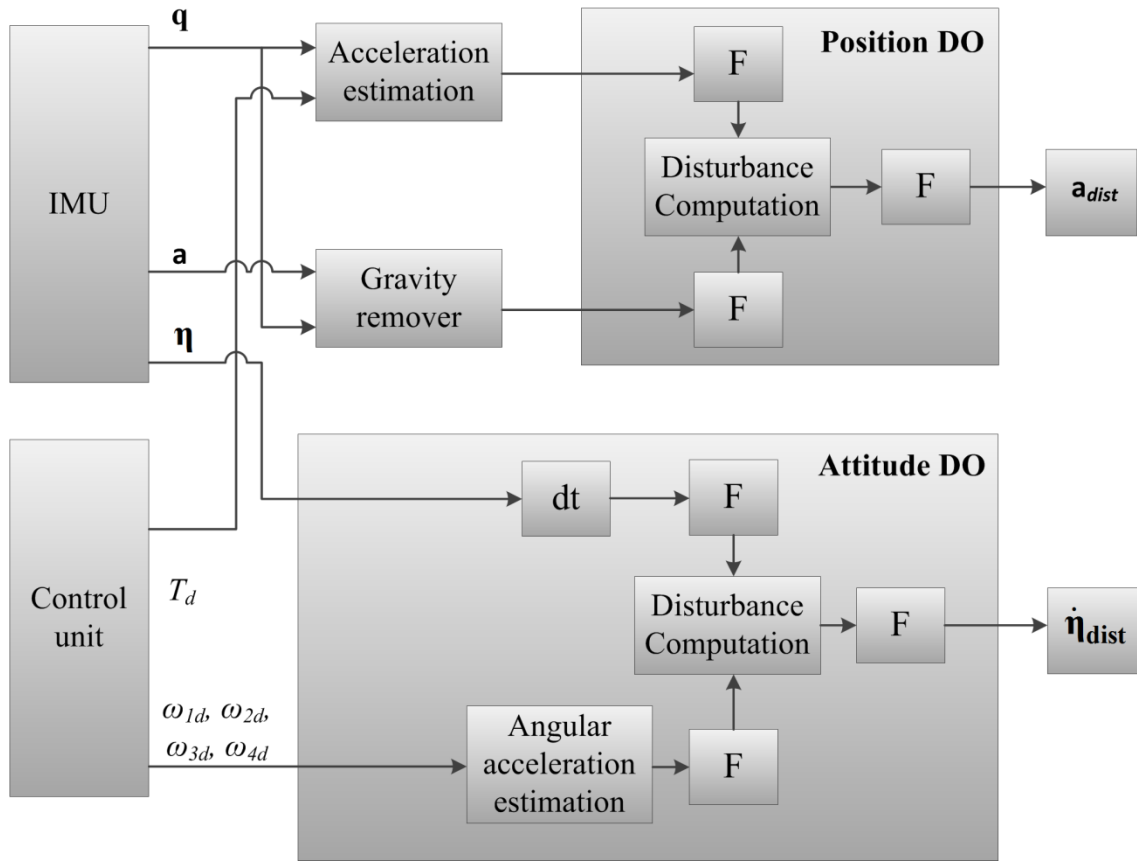


Figure 4.3 Block diagram of the proposed attitude and position disturbance observer.

## 5 Simulation

The previous chapter was dedicated to the design of attitude and position controllers for the quadrotor, namely backstepping, LQ and PD controllers. In this chapter, all above mentioned controllers are simulated and the performance of particular controller is evaluated using various quality indicators such as the integral of absolute error  $I_{AE}$ , the integral of absolute total thrust  $I_{AT}$  and settling times.

The attitude controller should meet some requirements, i.e. the regulation of the roll and the pitch angle should be significantly faster than a regulation of the yaw angle.

### 5.1 Simulation parameters and parameters of designed controllers

This section deals with the verification of the controllers designed in previous sections through a numerical simulation.

The non-linear model of the quadrotor from equation (1.9) and (1.10) was used to carry out all simulations. Several simulation conditions were adjusted in order to set the simulation closer to the reality. The sampling period of the simulation was set to 10 ms. All signals used to control the quadrotor were sampled at this rate, except the position, which is sampled at a frequency of 10 Hz. Furthermore, some restrictions related to the actuator were applied based on measurements done in [24]. The maximum angular speed of the actuator was set to  $650 \text{ rad}\cdot\text{s}^{-1}$  and the minimum to

150 rad·s<sup>-1</sup>. Also the delay of the actuators was implemented due to the use of the electronic speed controller (ESC).

Moreover, the sensor noise was implemented to the measured feedback signals. Gaussian noise with a variance of 10<sup>-6</sup> rad<sup>2</sup>·s<sup>-2</sup> was added to the angular velocity. The quaternion is computed from the angular velocity, therefore there is no need to add another noise particularly to the quaternion.

The position was deteriorated with Gaussian noise with a variance of 10<sup>-4</sup> m<sup>2</sup>.

The evaluation of the designed controllers was done under two conditions: a) disturbance free condition and b) constant wind condition. In both scenarios the quadrotor has to follow the same trajectory; firstly the quadrotor takes off to altitude of 1 m, then at time  $t = 15$  s flies from point  $[0 \ 0 \ 1]$  to the point  $[5 \ 5 \ 6]$  respect to inertial frame  $E_I$  and also rotates 90 degrees around the  $z$  axis. At time  $t = 20$  s it rotates back and at time  $t = 35$  s comes back to point  $[0 \ 0 \ 1]$  and lands at time  $t = 45$  s.

The quadrotor is an under-actuated system, i.e. all desired movement are interconnected and generated by actuators with performance restriction. The position has higher priority than the rotation around  $z$  axis; therefore the desired yaw angle was filtered by a low pass filter.

Table 1 shows the list of the chosen desired poles and corresponding gains for proportional and derivative components of the attitude PD controller.

Table 1. Components of attitude PD controller.

Output	$\lambda_1$	$\lambda_2$	$K_P$	$K_D$
$\tau_{xd}$	-21	-21	9.5256	0.9072
$\tau_{yd}$	-21	-21	9.5256	0.9072
$\tau_{zd}$	-15	-17	10.8360	1.3632

Chosen poles and corresponding gains for the proportional and derivative component of the trajectory tracking PD controller are listed in Table 2. The desired poles were chosen with respect to the connected attitude controller.

Table 2. Components of position PD controller.

Attitude controller	Output	$\lambda_1$	$\lambda_2$	$K_P$	$K_D$
PD+LQR	$u_x$	-25	-1	2.5484	2.6504
	$u_y$	-25	-1	-2.5484	-2.6504
	$T_d$	-9	-1.45	13.05	10.45
B	$u_x$	-28.5	-1	2.9052	3.0071
	$u_y$	-28.5	-1	-2.9052	-3.0071
	$T_d$	-10	-1.44	14.4	11.4

The calculated optimal regulator gain matrix  $\mathbf{K}_A$  of attitude controller is given by the following equation:

$$\mathbf{K}_A = \begin{bmatrix} 4.474 & 0 & 0 & 0.542 & 0 & 0 \\ 0 & 4.472 & 0 & 0 & 0.542 & 0 \\ 0 & 0 & 3.162 & 0 & 0 & 0.877 \end{bmatrix} \quad (5.1)$$

The calculated optimal regulator gain matrix  $\mathbf{K}_P$  of position controller is given by the following equation:

$$\mathbf{K}_P = \begin{bmatrix} 2.45 & 0 & 0 & 2.739 & 0 & 0 \\ 0 & -2.45 & 0 & 0 & -2.739 & 0 \\ 0 & 0 & 3.873 & 0 & 0 & 3.57 \end{bmatrix} \quad (5.2)$$

The value of the parameter  $c_{1A}$  is 35 and  $\mathbf{c}_{2A}$  is a diagonal matrix with vector [35 35 3] on the main diagonal.

The parameter  $\mathbf{c}_{1P}$  is diagonal matrix with the vector  $\mathbf{V}_{1P}$  on the main diagonal and similarly parameter  $\mathbf{c}_{2P}$  has the vector  $\mathbf{V}_{2P}$  on the main diagonal. The backstepping trajectory controller was tuned differently for the PD, LQR and the backstepping attitude controller. Chosen parameters are shown in Table 3.

Table 3. Components of position backstepping controller.

Attitude controller	$\mathbf{V}_{1P}$	$\mathbf{V}_{2P}$
PD	[1 1 3]	[1.75 1.75 1.5]
LQR	[1 1 3]	[1.85 1.85 1.5]
B	[1 1 3]	[2 2 1.5]

## 5.2 Trajectory tracking without the external disturbance

Various quality indicators are chosen to discuss the well-working and the efficiency of the proposed algorithms, such as the integral of absolute error  $I_{AE}$ , the integral of absolute total thrust  $I_{AT}$  and settling times. From the dynamics it is evident, that settling time related to the  $x$  and  $y$  axis should be the same for distancing as well as for approaching, but there is also change in the altitude, which can result in different settling times. For the mentioned reason the settling time for distancing and ascending  $t_{Sr}$  and also for approaching and descending  $t_{Sf}$  will be determined.

All combinations of attitude and position controllers were simulated and the results are shown in Table 4 and Table 5. The best value of each quality indicator is indicated by green colour and the worst value is indicated by red colour.

Table 4. Quality indicators of controller's performance: Integral of absolute errors and thrust.

Att+Pos	$I_{AE_x}$ [m·s]	$I_{AE_y}$ [m·s]	$I_{AE_z}$ [m·s]	$I_{AT}$ [N·s]
PD+PD	12.98	12.96	12.31	495.610
LQR+PD	<b>12.76</b>	<b>12.74</b>	12.13	495.578
B+PD	13.31	13.26	12.66	495.280
PD+LQR	13.69	13.54	<b>13.33</b>	495.084
LQR+LQR	13.35	13.26	13.15	495.098
B+LQR	<b>13.88</b>	<b>13.66</b>	13.71	<b>494.727</b>
PD+B	12.98	13.03	11.70	495.915
LQR+B	<b>12.75</b>	12.81	<b>11.57</b>	<b>495.989</b>
B+B	13.30	13.38	12.07	495.466

Table 5. Quality indicators of controllers' performance: Settling times.

Att+Pos	$t_{Sr_{xy}}$ [s]	$t_{Sf_{xy}}$ [s]	$t_{Sr_z}$ [s]	$t_{Sf_z}$ [s]
PD+PD	<b>3.2</b>	<b>2.65</b>	<b>2.00</b>	<b>3.7</b>
LQR+PD	<b>2.7</b>	2.90	<b>2.00</b>	<b>3.7</b>
B+PD	3.0	3.20	2.10	<b>3.7</b>
PD+LQR	3.5	<b>3.50</b>	<b>3.35</b>	<b>2.6</b>
LQR+LQR	3.1	3.35	3.30	2.7
B+LQR	3.1	3.30	3.30	2.7
PD+B	3.0	<b>2.65</b>	2.10	3.0
LQR+B	<b>2.7</b>	2.90	2.40	3.0
B+B	2.9	3.10	2.30	3.0

We can see that all proposed controllers are energetically approximately equally efficient. When comparing integrals of absolute error, the controllers with the PD and the backstepping position controller show better performance than controllers with the LQR position controller. Settling times are compared in the form of proportions. The worst performance corresponds to controllers with the LQR position controller, where settling time is from 1.4 to 1.6 times longer than the shortest settling time, excluding the settling time corresponding to descending of the quadrotor, which was the best achieved value. Controllers with the PD and the backstepping position controllers exhibit comparable behaviour. After considering all quality indicators, we chose the following controllers to be the best designed and tuned controllers of all the abovementioned controllers without the occurrence of the external disturbance: the LQR attitude controller in connection with the PD and the backstepping position controller, and the PD attitude controller with the backstepping position controller.

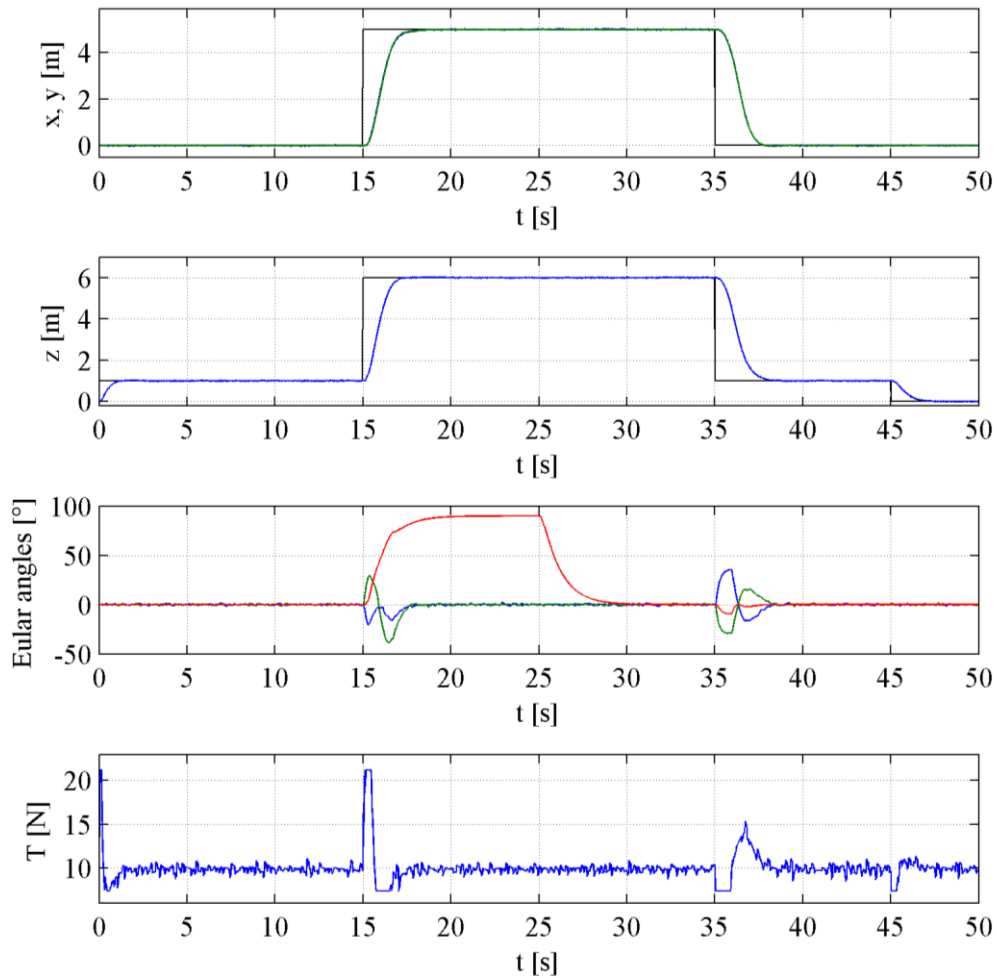


Figure 5.1 The performance of the controller comprised of the PD attitude and the backstepping position controller. At time  $t = 15$  s, the quadrotor is ordered to move 5 m in all axes and to rotate  $90^\circ$  around the  $z$  axis; at time  $t = 20$  s the quadrotor rotates back around the axis and at time  $t = 35$  s is ordered to come back to the initial position. The third subplot depicts the attitude of the quadrotor in terms of Euler angles, i.e. roll (blue line), pitch (green line) and yaw (red line).

Figure 5.1 highlights the performance of one of the best controllers, namely the PD attitude and the backstepping position controller. As can be seen in the figure below the quadrotor is ordered to move 5 m in all axes and to rotate  $90^\circ$  around the  $z$  axis at time  $t = 15$  s. The quadrotor reached the desired position in  $xy$  plane within 3 s while the altitude is reached earlier, i.e. under 2.1 s. The desired orientation is reached within 5 s because the position is assigned with a higher priority than a rotation around  $z$  axis. This behaviour can be seen in the third subplot depicting the attitude of the quadrotor in terms of Euler angles, i.e. roll (blue line), pitch (green line) and yaw (red line). The change in the yaw is interrupted at the time 16.7 s so that the quadrotor reached the desired position at the first. The quadrotor is ordered to rotate back around the  $z$  axis at time  $t = 20$  s. This command is executed within 4 s. The change in orientation only around the axis  $z$  is performed 1 s faster than when the quadrotor is also commanded to change its position. At time  $t = 35$  s the quadrotor is ordered to come back to the initial position. The position in the  $xy$  plane is reached within 2.65 s. The settling time of this change is shorter than the first command due to not performing the change in the orientation around the  $z$  axis.

The quadrotor descends at desired altitude within 3 s. The descending takes a little longer than ascending because the rotating propellers increases the aerodynamic drag when the quadrotor is moving in the opposite direction to the flow of the air generated by propellers.

### 5.3 Trajectory tracking with the occurrence of the external disturbance

The quadrotor often flies in an environment where external disturbances can occur. Therefore a verification of designed controllers is done under the presence of an external disturbance force. The desired trajectory remains the same as in previous section, but a force given by the vector  $[2 \ 2 \ -5]$  and expressed in [N] is applied at time  $t = 20$ s. The disturbance force then disappears at time  $t = 40$ s.

The quality indicators from the previous section are expanded by adding the settling time after the occurrence of the disturbance  $t_{SD}$ , the settling time after the disappearance of the disturbance  $t_{ED}$  and maximum overshoots in both mention cases  $O_{SD}/O_{ED}$ . The settling time for distancing and ascending  $t_{Sr}$  is the same as in previous case; hence only the settling time for approaching and descending  $t_{Sf}$  will be determined because they change due to the presence of the external disturbance.

All combinations of the attitude and the position controllers were simulated and the results in the form of quality indicators are listed in Table 6, Table 7 and Table 8. The best value of each quality indicator is indicated by green colour and the worst value is indicated by red colour.

As in the previous analysis, the proposed controllers are energetically very similar and combinations with the LQR position controllers reach the highest value of the integral of the absolute error.

Table 6. Quality indicators of controllers' performance: Integral of absolute errors and thrust.

<b>Att+Pos</b>	$I_{AE_x}$ [m·s]	$I_{AE_y}$ [m·s]	$I_{AE_z}$ [m·s]	$I_{AT}$ [N·s]
<b>PD+PD</b>	13.77	13.74	10.97	600.885
<b>LQR+PD</b>	13.63	13.57	11.02	600.740
<b>B+PD</b>	13.98	13.98	11.06	600.736
<b>PD+LQR</b>	14.33	14.16	12.63	600.444
<b>LQR+LQR</b>	14.07	13.95	12.67	600.310
<b>B+LQR</b>	14.55	14.35	12.94	599.981
<b>PD+B</b>	13.51	13.56	10.89	601.262
<b>LQR+B</b>	13.33	13.36	10.94	601.206
<b>B+B</b>	13.79	13.78	10.85	600.880

From results given by Table 7, it can be seen a dependency between the used attitude controller used and the value of the maximum overshoot in the  $xy$  plane. The best performance is achieved by using the backstepping attitude controller, a slightly worse one with the LQR attitude controller and the worst with the PD attitude controller.

Table 7. Quality indicators of controllers' performance: Maximal overshoots.

Att+Pos	$O_{SD_{xy}}$ [m]	$O_{ED_{xy}}$ [m]	$O_{SD_z}$ [m]	$O_{ED_z}$ [m]
<b>PD+PD</b>	<b>0.25</b>	<b>0.20</b>	<b>0.13</b>	0.13
<b>LQR+PD</b>	0.20	0.18	<b>0.13</b>	0.13
<b>B+PD</b>	<b>0.14</b>	<b>0.13</b>	<b>0.13</b>	<b>0.12</b>
<b>PD+LQR</b>	0.24	<b>0.20</b>	0.24	<b>0.24</b>
<b>LQR+LQR</b>	0.20	0.19	<b>0.25</b>	<b>0.24</b>
<b>B+LQR</b>	0.15	0.15	<b>0.25</b>	<b>0.24</b>
<b>PD+B</b>	0.23	<b>0.20</b>	0.20	0.20
<b>LQR+B</b>	0.18	0.18	0.20	0.20
<b>B+B</b>	<b>0.14</b>	<b>0.13</b>	0.20	0.20

Naturally, the maximum overshoot in the  $z$  plane depends only on the position controller. The smallest overshoot of 0.12 m was achieved by the PD position controller. The maximum overshoot created by controllers with the backstepping position controller was around 1.5 times higher than that, but the highest value was obtained by the LQR position controller.

The maximum overshoot is around the value of the 0.25 m but there is no need to come so close to any object because if the quadrotor is near the object the turbulences of recoil will affect the performance of the quadrotor. Moreover most of the available GNSS sensors possess the accuracy of 1m.

Almost all controllers manage to descend from 6 m to 1 m during the presence of the external disturbance without overshooting except the controller comprised of the backstepping attitude controller and the PD position controller. The maximum value of this overshoot was 0.4 m that is undesired behaviour especially when we take into consideration the possibility of the landing.

Table 8. Quality indicators of controllers' performance: Settling times.

Att+Pos	$t_{SD_{xy}}$ [s]	$t_{ED_{xy}}$ [s]	$t_{SD_z}$ [s]	$t_{ED_z}$ [s]	$t_{sf_{xy}}$ [s]	$t_{sf_z}$ [s]
<b>PD+PD</b>	2.1	1.90	<b>1.50</b>	<b>1.25</b>	2.70	<b>3.50</b>
<b>LQR+PD</b>	2.1	1.95	<b>1.50</b>	1.30	2.95	<b>3.50</b>
<b>B+PD</b>	1.9	<b>1.80</b>	<b>1.50</b>	1.30	3.40	3.00*
<b>PD+LQR</b>	<b>2.3</b>	1.90	2.20	1.90	<b>3.60</b>	2.25
<b>LQR+LQR</b>	<b>2.3</b>	<b>2.00</b>	2.20	<b>2.00</b>	3.40	2.70
<b>B+LQR</b>	1.9	1.90	<b>3.00</b>	<b>2.00</b>	3.10	<b>2.00</b>
<b>PD+B</b>	2.0	1.85	1.70	1.70	<b>2.65</b>	2.50
<b>LQR+B</b>	1.9	1.90	1.70	1.70	2.90	2.60
<b>B+B</b>	<b>1.8</b>	<b>1.80</b>	2.25	1.70	3.10	2.80

The settling time of the deviation of the position caused by external disturbance is slightly longer when the LQR position controller is used. Settling times of the rest of the controllers are comparable to each other. In general all controllers show sufficient behaviour when it comes to settling time since all controllers returned to the original position within a relatively short time, i.e. under 3 s. Therefore in this case the amplitude of the overshoots is more important parameter to look at.

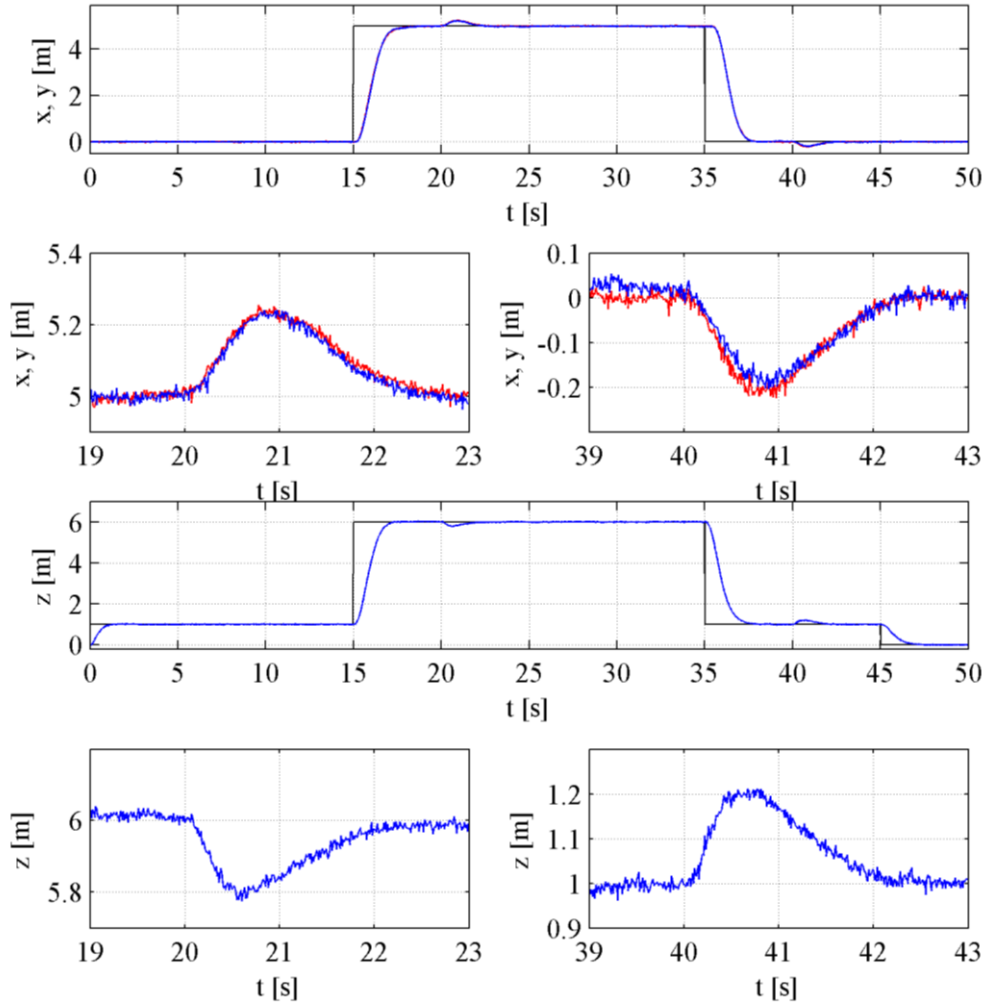


Figure 5.2 The performance of the controller comprised of the PD attitude and the backstepping position controller. The desired trajectory is the same as in previous section and the disturbance force given by the vector  $[2 \ 2 \ -5]$  is applied at time  $t = 20$  s and it disappears at time  $t = 40$  s.

Taking into account all quality indicators, we consider the best combinations to be the backstepping attitude controller in connection with the PD and the backstepping position controller, and the combination of the PD attitude controller and the backstepping position controller of quadrotor. While processing the results of all controllers' performance we took into account two best values for each quality indicator and the chosen controllers were those that had the highest number of best values.

The performance of the PD attitude and the backstepping position controller is depicted in Figure 5.2. The desired trajectory and the performance during the first 20 s is the same as in previous section. As can be seen in the figure below the disturbance force given by the vector  $[2 \ 2 \ -5]$  is applied at time

$t = 20$  s. As the result of the disturbance the quadrotor position was changed. The overshoot in the  $xy$  plane was equal to 0.23 m and the change in the altitude was equal 0.2 m. The DO identified the applied disturbance forces and reached the original position in 2 s in the  $xy$  plane and the altitude was restored in 1.7 s. The quadrotor is ordered to come back to the initial position at time  $t = 35$  s while the disturbance is still acting on the quadrotor. The position in the  $xy$  plane is reached within 2.65 s. The quadrotor descends at desired altitude within 2.5 s. The disturbance forces disappeared at the time  $t = 40$  s. The overshoot in all axes was equal to 0.2 m. The DO identified the disappearance of disturbance forces and the quadrotor reached the original position in 1.85 s in the  $xy$  plane and the altitude was restored in 1.7 s.

## 6 Experimental results

This chapter outlines various steps that must be done for the verification of proposed attitude controller using a real platform. Firstly we will discuss usage of all devices connected to the control board. Then some part of the first subchapter will be dedicated to the source code itself in the form of the flowchart. Secondly the application used to log data and send commands to the real platform will be discussed. Finally designed attitude controllers will be implemented and verified using real platform mounted into the test stand.

### 6.1 Implementation of control algorithm into real platform

The chosen platform for the implementation of control algorithms was quadrotor DJI F450. The platform by DJI company consists of a main frame, 30A OPTO ESCs and motors 2212/920KV. To be able to fly this platform several others components must be added, namely LiPo battery, control unit, DC/DC converter, IMU and Bluetooth device.

Figure 6.1 shows all abovementioned components and their interconnections. The control unit should maintain control, mathematical and other important operations. The discovery platform with powerful microcontroller ST32F4, which runs at 168MHz rate, was chosen. The control unit was powered by the LiPo battery via 5 V Step-down converter that transforms battery voltage to necessary voltage of 5 V. The IMU MPU9150 was used to measure angular speed in the body-fixed frame  $E_B$ . The IMU is able to measure all angular speeds and linear acceleration every 1 ms. The orientation from magnetometer is possible to read every 7 ms. The I<sup>2</sup>C serial bus is used for communication between the control unit and the IMU.

The Bluetooth device RN-42 is used to exchange data between the control unit and an external device such as computer. The ESCs acquires PWM from the digital outputs (DOut) of the control unit and transforms this signal into 3-phase power waveform that makes the motor to rotate at specific angular speed.

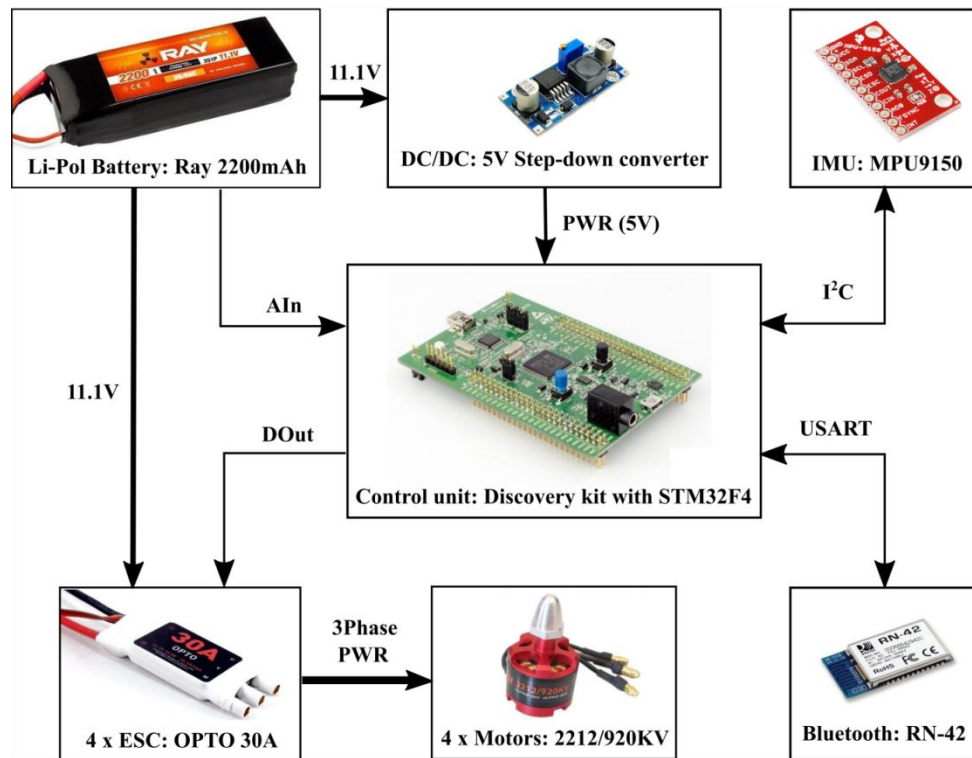


Figure 6.1 Scheme of all peripherals connected to the control board.

## 6.2 HMI for data collection and command execution

An application depicted in Figure 6.2 was created using C# language and it serves as the interface between operator and the flying platform (Section A). This application also is performing the function of being the interface to the test stand used to verify the proposed attitude control algorithms (Section B). This application was also used to tune all designed attitude controllers (Section C). The main purpose of the application is to control and monitor the behaviour of the real platform.

## 6.3 Verification of proposed control algorithms

This subchapter highlights data read directly from the quadrotor mounted in the designed test stand discussed in chapter 2.2. The data was read using the PC application described in the previous subchapter 6.2.

The controller parameters had to be newly tuned because when parameters from chapter 5.1 were applied the quadrotor shows unstable behaviour. There can be various reasons why it is so. The dynamics of the test stand and its lack of rigidity can have considerable impact on the quadrotor performance. Moreover some parameters used in the mathematical model may not be accurate. The example of such parameters can be the motor constants, because bearings of the motors are probably worn in the moment of the data reading. In addition the dynamics only of one motor were identified. Further when the identification was made only one motor was connected to the battery at that time, so there is high possibility that used battery cannot supply all motors with required current.

The implemented designed attitude controllers will be evaluated by tracking desired sequence of orientation.

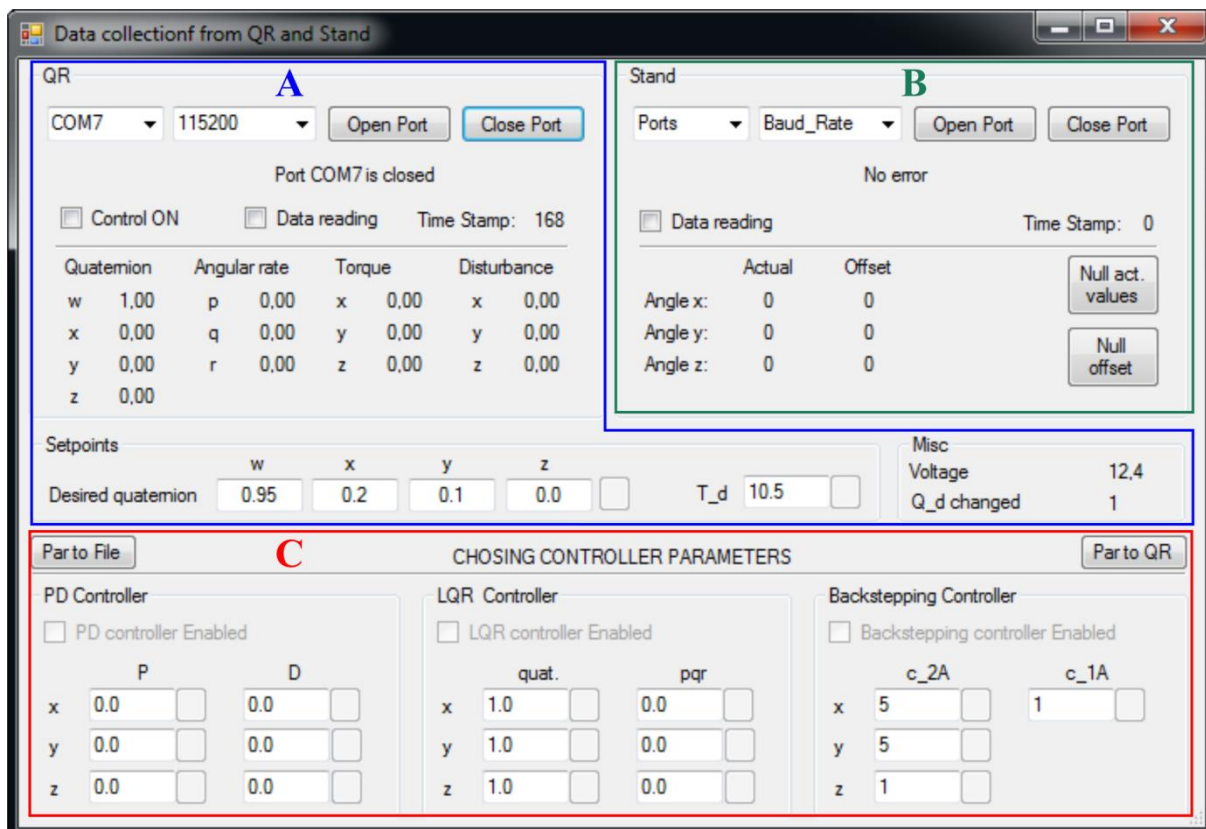


Figure 6.2 Application used to log data and send commands to the real platform.

### 6.3.1 Parameters of designed controllers applied to real platform

Parameters for each axis were tuned separately. The first tuned parameters were parameters related to  $z$  axis, followed by the parameters of  $x$  axis. The last tuned parameters were those of  $y$  axis.

Firstly proportional parameters of the PD controller were identified. The derivative parameter was set to 0 and the proportional part of the controller was increased step by step until the quadrotor starts to oscillate around the particular axis. Then the 80 % of the value was set to be the proportional part of the PD controller. The derivative part of the PD controller was increased until the settling time of the quadrotor was around 1-2 s.

Table 9 shows the list of the chosen corresponding gains for proportional and derivative components of the attitude PD controller.

Table 9. Components of attitude PD controller.

Output	$K_P$	$K_D$
$\tau_{xd}$	1.34	0.3
$\tau_{yd}$	1.34	0.3
$\tau_{zd}$	0.6	0.3

The LQR controller was tuned in the similar way as the PD controller. Firstly the elements of gain matrix  $K_A$  that correspond to the quaternion were tuned. Subsequently, the elements of the gain matrix

$K_A$  corresponding to angular velocity of the quadrotor were identified. The regulator gain matrix  $K_A$  of LQR controller is given by equation (6.1).

$$K_A = \begin{bmatrix} 1.34 & 0 & 0 & 0.3 & 0 & 0 \\ 0 & 1.34 & 0 & 0 & 0.3 & 0 \\ 0 & 0 & 0.6 & 0 & 0 & 0.3 \end{bmatrix} \quad (6.1)$$

The parameters of the backstepping controller were tuned as followed: the value of the parameter  $c_{1A}$  is 10 and  $c_{2A}$  is a diagonal matrix with vector  $[11 \ 11 \ 3]$  on the main diagonal. The parameters of backstepping controllers were obtained the similar way as the parameters of the PD and LQR controller. That means the first tuned parameter was  $c_{1A}$  which corresponds to the attitude of the system and then the vector  $c_{2A}$  related to angular velocity of quadrotor was identified.

### 6.3.2 Tracking desired sequence of orientation

This subchapter shows the performance of designed controllers when the quadrotor should follow predefined sequence of the required setpoints of the orientation. Firstly the desired sequence will be outlined. Secondly the performance of all controllers will be shown. Finally some of quality indicators will be used to make comparison between implemented control techniques.

The sequence of required setpoints of orientation is depicted in Figure 6.3 using quaternion representation of orientation. The sequence is divided into 18 sections.

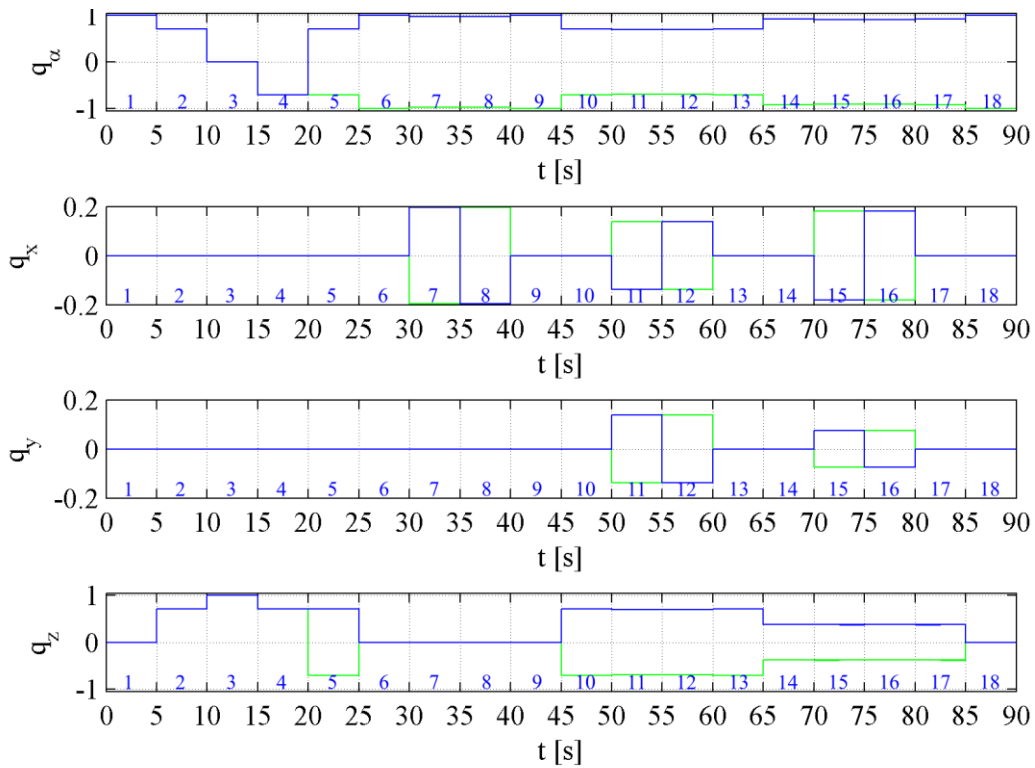


Figure 6.3 Sequence of desired orientation represented using quaternion.

Quaternion represents the rotation of the object with the respect to initial orientation. The rotation as we know can be executed in two ways, i.e. clockwise rotation or counter-clockwise rotation. The

rotation of  $360^\circ$  around any axis is represented by following quaternion  $q = [-1 \ 0 \ 0 \ 0]$ . Because of abovementioned reasons the Figure 6.3 contains two sequences (blue and green line) representing the same orientation of the quadrotor.

The performances of designed controllers, i.e. PD, LQR and backstepping controller are outlined in following figures: Figure 6.4, Figure 6.5 and Figure 6.6, respectively. Figures depict the actual quaternion represented by blue line, quaternion error represented by green line and the desired quaternion represented by red and magenta line.

Change in setpoint around  $z$  axis also influences the rest of the axes which is given by the computation of the quaternion error. The change in the orientation around  $z$  axis causes the change of the quaternion error around all axes.

The performance of the **PD attitude controller** is depicted in Figure 6.4, where the change of the orientation of the quadrotor during the performance of the sequence is shown.

The trajectory around  $z$  axis coincides with the desired trajectory, but the trajectory around  $x$  and  $y$  axis suffers from the permanent deviation and oscillation. This behaviour can be caused by the lack of the rigidity of the test stand in both  $x$  and  $y$  axis. The rotation in both problematic axes is provided by carbon tubes of almost 1m of length which end in flexible polymer parts. Therefore the performance of the controller is affected by the mechanical oscillation of the designed test stand. The movement in  $z$  axis is not affected because rotation point around  $z$  axis of the test stand coincides with the rotation point of the quadrotor.

The settling time of the desired orientation in  $x$  and  $y$  axis is mostly less than 1 s when permanent deviation is neglected. The slower performance of the  $z$  axis is required because of the lower importance of control of the orientation around this axis.

The performance of the **LQR attitude controller** is depicted in Figure 6.5 where the change of the orientation of the quadrotor during the performance of the sequence is shown. The trajectory around  $z$  axis coincides with the desired trajectory, but the trajectory around  $x$  and  $y$  axis suffers from the permanent deviation and oscillation. The cause of these phenomes is the non-rigidity of the test stand. The effect of the test stand was explained previously when evaluating the performance of the implemented PD controller.

The settling time of the desired orientation in  $x$  and  $y$  axis is mostly less than 1 s when permanent deviation is neglected. The slower performance of the  $z$  axis is required because of the lower importance of control of the orientation around this axis.

The performance of the **backstepping attitude controller** is depicted in Figure 6.6 where the change of the orientation of the quadrotor during the performance of the sequence is shown. The trajectory around  $z$  axis coincides with the desired trajectory, but the trajectory around  $x$  and  $y$  axis suffers from the permanent deviation and oscillation. The cause of this phenomenon is the non-

rigidness of the test stand. The effect of the test stand was explained previously when evaluating the performance of the implemented PD controller.

Performances of all implemented controllers contain very similar oscillation and deviation around  $x$  and  $y$  axis, which supports presented theory about the source of the oscillation and also deviation.

The settling time of the desired orientation in  $x$  and  $y$  axis is mostly less than 1 s when permanent deviation is neglected. The slower performance of the  $z$  axis is required because of the lower importance of control of the orientation around this axis.

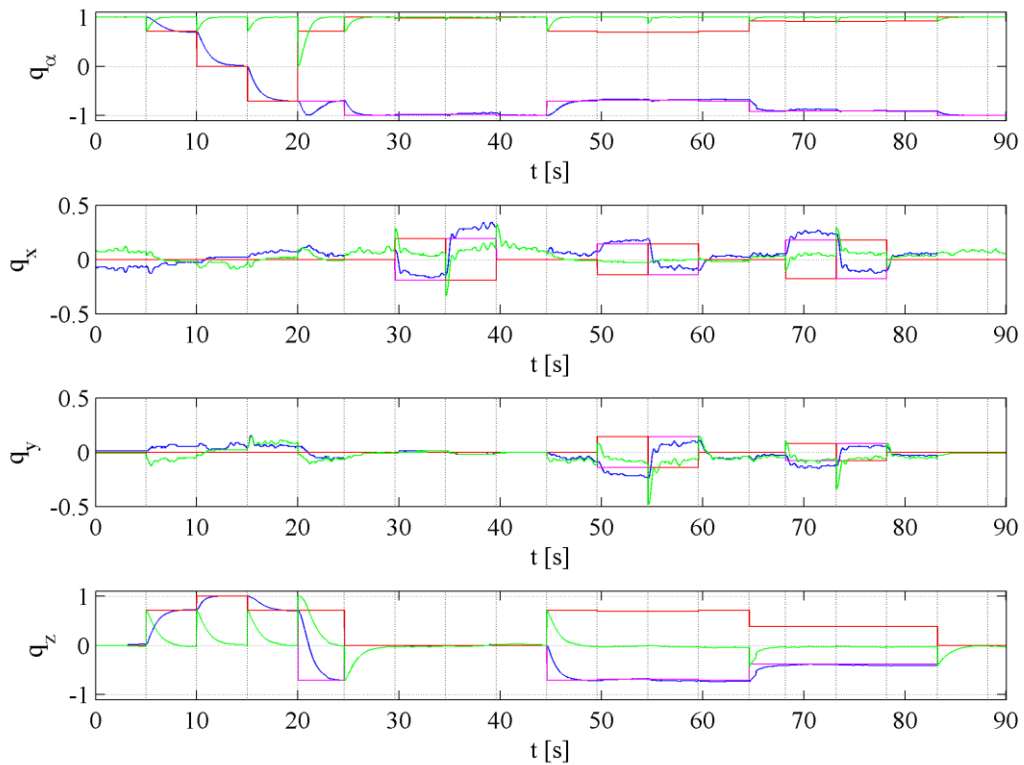


Figure 6.4 Performance of the sequence using PD controller expressed by various quaternions, such as actual quaternion (blue line), quaternion error (green line) and desired quaternion (red and magenta line).

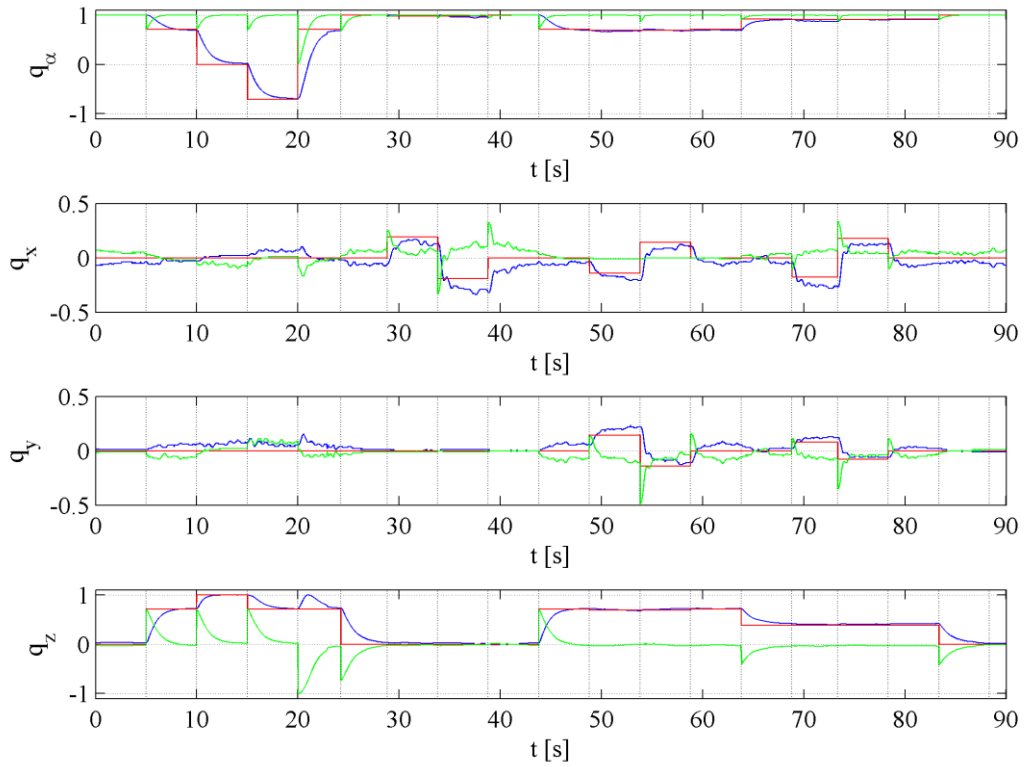


Figure 6.5 Performance of the sequence using LQR controller expressed by various quaternions, such as actual quaternion (blue line), quaternion error (green line) and desired quaternion (red and line).

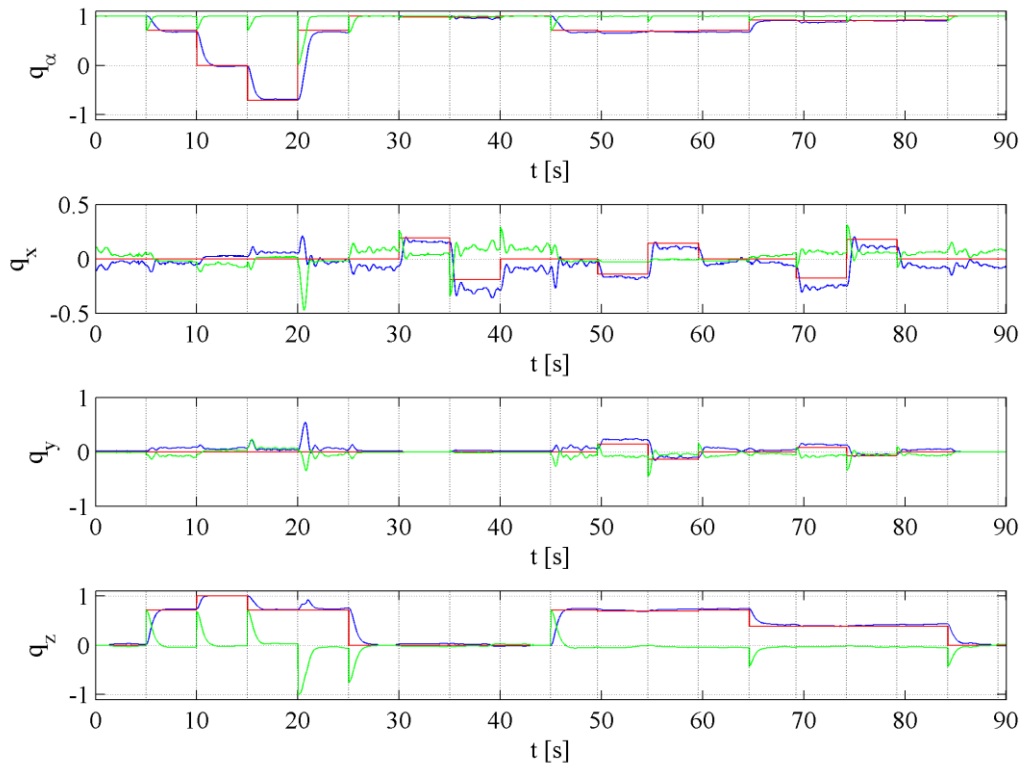


Figure 6.6 Performance of the sequence using backstepping controller expressed by various quaternions, such as actual quaternion (blue line), quaternion error (green line) and desired quaternion (red and line).

Various quality indicators are chosen to discuss the well-working and the efficiency of the proposed algorithms, such as the integral of absolute error  $I_{AE}$ , integral of absolute desired torque  $I_{AM}$  and maximum absolute variation of the quaternion  $O_q$ .

Table 10 shows the overview of quality indicators list in abovementioned tables. The sequence is divided into 18 particular sections, where each section corresponds to one desired setpoint of the attitude of the quadrotor. Chosen quality indicators are identified separately for each section. Table 10 depicts the total number of the best and also the worst performance related to the particular quality indicator.

The best value of each quality indicator for entire sequence is indicated by green colour and the worst value is indicated by red colour.

Table 10 Overview of quality indicators of controllers' performance.

	PD		LQR		Backstepping	
	The best	The worst	The best	The worst	The best	The worst
$I_{AE}$		---			---	
$I_{AM}$ [N·m·s]			---			---
$I_{AE\alpha}$	5	7	1	5	12	6
$I_{AE_x}$	6	5	9	2	3	11
$I_{AE_y}$	4	5	10	2	4	11
$I_{AE_z}$	3	6	5	6	10	6
$I_{AM_x}$ [N·m·s]	5	8	11	3	2	7
$I_{AM_y}$ [N·m·s]	5	7	9	1	4	10
$I_{AM_z}$ [N·m·s]	7	0	9	4		14
$O_{q\alpha}$	13	3	13	2	7	9
$O_{q_x}$	6	4	11	4	5	11
$O_{q_y}$	6	7	13	2	5	11
$O_{q_z}$	10	4	11	7	7	9
<b>Sum</b>	56	70	102	38	61	105
<b>Total</b>	3	2	8	2	2	8

The evaluation of the performed sequences of chosen controllers can be done in two different ways.

The first approach to evaluate achieved results and to compare the performance of the controllers is to focus mainly on the reaching the desired orientation in the shortest possible time omitting the importance of the efficiency of power supply. The integral of total absolute quaternion error and the maximal absolute quaternion variation are decisive quality indicators used in this approach. The backstepping controller reports the smallest value of the sum of all parts of the quaternion error and

also the best control around  $z$  axis, but when it comes to control around  $x$  and  $y$  axis this controller exhibits the worst results. The best attitude control around  $x$  and  $y$  axis achieved the LQR controller. The PD controller shows average performance when only considering the integral of total absolute quaternion error and maximal absolute quaternion variation as quality indicators. To sum up, the LQR attitude controller is considered to be the best option when taking into account only the importance of reaching the desired quaternion as fast as possible.

The second approach focuses not only on reaching desired orientation but also on the efficiency of the power supply. The second approach expands the quality indicator from first approach with the total absolute desired torque. The most energy efficient controller is the LQR controller which consumed the least energy during all sequence. When the movement is divided into various rotations related to the particular axis, the LQR controller is the most efficient controller around  $x$  and  $y$  axis while around  $z$  axis the most efficient controller is PD controller. The backstepping controller consumes the most from power supply among implemented controllers. When taking into account the energy consumption and also the quaternion error, the best performance exhibits the LQR controller and the worst performance shows the backstepping controller. As in the previous case, the PD controller exhibits average performance.

As can be seen in Table 10, the best performance with respect to chosen quality indicators exhibits implemented LQR controller. The worst performance with respect to chosen quality indicators demonstrates implemented backstepping controller. The PD controller shows average performance.

## **Conclusion**

In this thesis different control methods were used to designed attitude and also position controllers, namely the PD, the LQR and the backstepping control techniques. All controllers use the quaternion representation of the attitude. The output of position controllers is the desired quaternion and the desired thrust of quadrotor. The attitude controllers use calculated quaternion error to compute desired torques.

Moreover an estimator of the linear velocity and the position along with a disturbance observer was designed to improve trajectory tracking under the presence of an external disturbance.

Two scenarios were proposed to verify all combination of attitude and position controllers. The first one was following the desired trajectory, where the movement along all axes and also the rotation around the  $z$  axis was ordered. The occurrence of an external disturbance was added in the second scenario.

In order to set the simulation closer to the reality some modifications were made, namely the consideration of actuator restrictions, the different sampling for feedback signals and the addition of noise to all feedback signals.

Several parameters used in simulation were obtained using the proposed test bed. The test bed allows us to identify the static and also the dynamic characteristics of the actuator. Knowledge of the dynamics of the actuator can help design a controller, which would be able to reduce power consumption and improve the control of the actuator and with it the whole quadrotor.

The quality indicators were chosen in order to be able to compare the performance of all controllers. Some of controllers exhibit very similar behaviour, so we choose three best controllers for each scenario. The only controller overlapping both scenarios was the PD attitude controller in connection with the backstepping position controller.

Designed attitude controllers were implemented into microcontroller on the control board of the real quadrotor. The application for PC was created to send commands and acquire data from the control board. Data between PC and the control board were transferred via Bluetooth.

The attitude controllers were verified using proposed test stand. The test stand works well in case of safety and measuring orientation. As we found out the test stand influenced the performance of the quadrotor not only with additional moment of inertia but also adds oscillations caused by low rigidity of used materials. The performance of controllers was evaluated using various quality indicators, such as the integral of absolute quaternion error, integral of absolute desired torque and the maximum absolute variation of the quaternion.

The best performance with respect to chosen quality indicators exhibited implemented LQR controller. The worst performance with respect to chosen quality indicators demonstrated implemented backstepping controller.

## **Main contribution of the dissertation thesis**

One of the contributions is the design and construction of the test bed and test stand. The test bed is used to experimentally identify parameters of the actuator and also to verify controllers designed to control the particular actuator. The test stand is used to verify and evaluate control algorithm used to control attitude of the quadrotor.

This design of the stand has various advantages in comparison with the stand currently on the market. The main advantage of the stand is that the tested VTOL can rotate in all 3 axes without restriction. We also used an absolute rotary position sensor for the measurement of the orientation. This type of the sensor do not suffer from the drift and provide us with the absolute orientation of the tested VTOL that means that the stand can also be used to calibrate IMU sensor mounted on the VTOL. The test stand was issued the certificate of registration of utility model no. 7766.

Despite the interest in quadrotor control techniques, no one, as far as we know, has compared various types of linear and non-linear attitude and position controllers with the use of a disturbance observer. Most studies have only focused on the comparison of attitude controllers or of position

controllers using the same attitude controller. Only a few works implemented a disturbance observer. These results were partially published in 2015 in the journal *Robotics and Autonomous System* with impact factor 1.618, i.e. the work has already been reviewed by various good reviewers.

Moreover, the position and linear velocity estimator is designed due to the different sampling periods of the feedback signals and the control loop, and the noise corruption of the feedback signals.

This paper also calls into question an assumption that non-linear controllers exhibit better performance when the external disturbance is present or the implementation of the disturbance observer to linear controllers is sufficient.

## References

- [1] X. Huo, M. Huo, H.R. Karimi. Attitude stabilization control of a quadrotor UAV by using backstepping approach. In *Math. Probl. Eng.*, 2014, pp. 1–9.
- [2] E. Fresk, G. Nikolakopoulos. Full quaternion based attitude control for a quadrotor, In *Proc. ECC*, Zürich, CH, 2013, pp. 3864–3869.
- [3] A. Alaimo, V. Artale, C. Milazzo, A. Ricciardello, L. Trefiletti. Mathematical modeling and control of a hexacopter, In *Proc. ICUAS*, Atlanta, USA, 2013, pp. 1043–1050.
- [4] E. Reyes-Valeria, S. Camacho-Lara, J. Guichard. LQR control for a quadrotor using unit quaternions: Modeling and simulation, In *Proc. CONIELECOMP*, Cholula, MX, 2013, pp. 172–178.
- [5] A. Zulu, S. John. A review of control algorithms for autonomous quadrotors, *Open J. Appl. Sci.*, 2014, vol. 4, pp. 547–556.
- [6] Rinaldi, F., Chiesa S., Quagliotti F.: Linear Quadratic Control for Quadrotors UAVs Dynamics and Formation Flight. In *Journal of Intelligent & Robotic Systems*. ISSN 1573-0409, 2013, vol. 70, no.1-4, pp. 203-220.
- [7] De Lellis Costa de Oliveira M. *Modeling, Identification and Control of a Quadrotor Aircraft*. Prague: Faculty of Electrical Engineering Czech Technical University in Prague, 2011. 52s. Master's thesis.
- [8] Mahony R., Kumar, V., Corke P. Multirotor Aerial Vehicles: Modeling, Estimation, and Control of Quadrotor. In *IEEE Robotics & Automation Magazine*, ISSN 1070-9932, 2012, vol. 19, no. 3, pp. 20-32.
- [9] Derafa, L., Madani, T., Benallegue, A. Dynamic modelling and experimental identification of four rotors helicopter parameters. In *Proc. IEEE International Conference on Industrial Technology*. Mumbai, India, 2006, pp. 1834-1839.

- [10] Bouabdallah, S. Design and control of quadrotors with application to autonomous flying. Tlemcen, Algeria: University of Abou Bekr Belkaïd, 2007. 129s. Dizertačná práca.
- [11] Leishman, J.G. *Principles of Helicopter Aerodynamics*. 2.vyd. Cambridge, MA: Cambridge University Press, 2006. 864s. ISBN 9780521858601.
- [12] Luukkonen, T. *Modelling and control of quadcopter*. Espoo: Aalto University, 2011. 26 s. Výskumný projekt v oblasti aplikovanej matematiky.
- [13] Bouadi, H., Simoes Cunha, S., Drouin, A., Mora-Camino, F. Adaptive sliding mode control for quadrotor attitude stabilization and altitude tracking. In *Proc. 12th IEEE international symposium on computational intelligence and informatics (CINTI 2011)*. Budapest, Hungary, 2011, pp. 449-455.
- [14] Amir, M.Y., Abbass, V. Modeling of quadrotor helicopter Dynamics. In *Proc. International Conference on Smart Manufacturing Application (ICSMA 2008)*. Gyeonggi-do, South Korea, 2008, pp. 100-105.

## Overview of author's publications

### ADC Publications in foreign current magazines

CHOVANCOVÁ, Anežka - FICO, Tomáš - HUBINSKÝ, Peter - DUCHOŇ, František. Comparison of various quaternion-based control methods applied to quadrotor with disturbance observer and position estimator. In *Robotics and Autonomous Systems*. Vol. 79, (2016), s. 87-98. ISSN 0921-8890. V databáze: SCOPUS: 2-s2.0-84958581863 ; CC: 000374358500007.

Cited by:

Farid G., Hongwei M., Ali S., Liwei Q. A review on linear and nonlinear control techniques for position and attitude control of a quadrotor, In *Control and Intelligent Systems*, 2017, vol. 45(1).

Guerrero M. E., Abaunza H., Castillo, P., Lozano R., & García C. D. Quadrotor Energy-Based Control Laws: a Unit-Quaternion Approach. In *Journal of Intelligent & Robotic Systems*, 2017, pp. 1-31.

Guerrero-Sanchez M., et al. Passivity-based control for a micro air vehicle using unit quaternions, In *Applied Sciences*, (Switzerland), 2017, vol. 7 (1).

Guerrero M. E., Abaunza H., Castillo, P., Lozano R., & García C. D. Energy based control for a quadrotor using unit quaternions. In *IEEE International Conference on Unmanned Aircraft Systems (ICUAS)*, 2016, pp. 144-151.

### ADF Publications in other national magazines

CHOVANCOVÁ, Anežka - RODINA, Jozef - HUBINSKÝ, Peter. Modelling of the VTOL Micro Aerial Mobile Robot. In *ATP Journal plus*. Č. 1 : Modelling of Mechanical and Mechatronic Systems (2012), s.104-107. ISSN 1336-5010.

## AFD Published papers at national scientific conferences

FICO, Tomáš - DUCHOŇ, František - CHOVANCOVÁ, Anežka - SPIELMANN, Róbert. Mechatronic concepts of automated weather radars (a survey). In *Procedia Engineering [elektronický zdroj] : The 6th International Conference on Modelling of Mechanical and Mechatronic Systems MMaMS 2014, 25-27 November 2014, Vysoké Tatry, Slovakia*. Vol. 96, (2014), p. 101-110. ISSN 1877-7058.

GURÁŇ, Matej - FICO, Tomáš - CHOVANCOVÁ, Anežka - DUCHOŇ, František - HUBINSKÝ, Peter - DÚBRAVSKÝ, Jozef. Localization of iRobot Create Using Inertial Measuring Unit. In *RAAD 2014 [elektronický zdroj] : 23rd International Conference on Robotics in Alpe-Adria-Danube Region. Conference Proceedings. September 3-5, 2014, Smolenice Castle, Slovakia*. 1. vyd. Bratislava : Publishing House of Slovak University of Technology, 2014, CD-ROM, [7] ISBN 978-80-227-4219-1.

### Cited by:

Pitale A., Bendre A., Jadhav P., Agashe R. Signal conditioning algorithms on accelerometers in an Inertial Navigation System (INS), In *Proc. International Conference on Signal and Information Processing (IconSIP)*, 2016, pp. 1-4.

Dang Y., Xu W. Calibration of iRobot create using UMBmark, In *Proc. 2016 IEEE 14th International Workshop on Advanced Motion Control (AMC)*, 2016, pp. 97-102.

CHOVANCOVÁ, Anežka - FICO, Tomáš. Design of a test bed for parameter identification of actuator used in quadrotors. In *ELITECH'14 [elektronický zdroj] : 16th Conference of Doctoral Students; Bratislava, Slovakia, 4 June 2014*. 1.vyd. Bratislava : Nakladateľstvo STU, 2014, CD-ROM, [6] p. ISBN 978-80-227-4171-2.

CHOVANCOVÁ, Anežka - FICO, Tomáš - CHOVANEC, Ľuboš - HUBINSKÝ, Peter. Mathematical Modelling and Parameter Identification of Quadrotor (a survey). In *Procedia Engineering [elektronický zdroj] : The 6th International Conference on Modelling of Mechanical and Mechatronic Systems MMaMS 2014, 25-27 November 2014, Vysoké Tatry, Slovakia*. Vol. 96, (2014), p. 172-181. ISSN 1877-7058.

### Cited by:

Meng X., et.al. Design and implementation of rotor aerial manipulator system, In *Proc. 2016 IEEE International Conference on Robotics and Biomimetics (ROBIO)*, 2016, pp. 673-678.

He Y., et al. Acceleration-based multiple-loop control of unmanned quadrotors with disturbances, In *Proc. 2016 IEEE Chinese Guidance, Navigation and Control Conference (CGNCC)*, 2016, pp. 1299-1304.

Yusuf Y., Agung H. Optimizing ultrasonic and barometric sensors for quadcopter's altitude-hold using YoHe V1.2 PID and KK V2.0 boards, In *Proc. 2016 International Seminar on Sensors, Instrumentation, Measurement and Metrology (ISSIMM)*, 2016, pp. 37-42.

Yie Y., Solihin M., Kit A. Development of swarm robots for disaster mitigation using robotic simulator software, In *Proc. 9th International Conference on Robotic, Vision, Signal Processing and Power Applications*, 2017.

Filho J., et.al. Modeling, Test Benches and Identification of a Quadcopter, In *Proc. 2016 XIII Latin American Robotics Symposium and IV Brazilian Robotics Symposium (LARS/SBR)*, 2016, pp. 49-54.

PALKOVIČ, Lukáš - RODINA, Jozef - CHOVANEC, Ľuboš - CHOVANCOVÁ, Anežka - HUBINSKÝ, Peter. Remote Laboratory with Modular Inertial Measuring Unit Platform. In *Procedia Engineering [elektronický zdroj] : The 6th International Conference on Modelling of Mechanical and Mechatronic Systems MMaMS 2014, 25-27 November 2014, Vysoké Tatry, Slovakia*. Vol. 96, (2014), p. 345-354. ISSN 1877-7058.

#### **AGJ Copyright certificates, patents, discoveries**

CHOVANCOVÁ, Anežka - FICO, Tomáš. *Zariadenie na testovanie VTOL platforiem : Úžitkový vzor č. 7766, Dátum o zápise ÚV : 24.3.2017, Vesník ÚPV SR č. 5/2017*. Banská Bystrica : Úrad priemyselného vlastníctva SR, 2017. 14 s.